Low Temperature Physics/Fizika Nizkikh Temperatur, 2021, vol. 47, No. 3, pp. 201–218

Molecular structure and vibrational spectra of isolated nucleosides at low temperatures

(Review Article)

A. Yu. Ivanov and S. G. Stepanian

B. Verkin Institute for Low Temperature Physics and Engineering of the National Academy of Sciences of Ukraine
Kharkiv 61103, Ukraine
E-mail: ivanov@ilt.kharkov.ua

Received November 16, 2020, published online January 26, 2021

The application of various action spectroscopy and absorption spectroscopy methods for studying the structure of biological molecules and their constituent fragments in an isolated state is considered. The main attention is paid to the results achieved in the study of the nucleosides which are the structural units of DNA and RNA. It has been demonstrated that modern low-temperature spectroscopy methods allow registration the vibrational spectra of isolated nucleosides in neutral or ionized form. It was shown that most of the nucleosides can be converted into the gas phase by prolonged evaporation from the Knudsen cell without thermal decomposition. Cooling molecules to cryogenic temperatures plays an important role in these studies. The conformational equilibrium of the gas phase between *syn* and *anti* subsets of nucleosides is maintained due to fast cooling when frozen in inert matrices. Within these subsets, interconversion processes between conformers can occur during cooling if the conformers are separated by low energy barriers. In inert gas matrices at 6 K, subsets of the *syn*-conformers of deoxyribonucleosides are mainly frozen with the C2′-endo structure of the deoxyribose ring. The structures of molecular ions of nucleosides are very different from their neutral forms. In particular protonation leads to the domination of the enol forms of thymidine, as well as *syn*-conformations of adenosine, stabilized by the intramolecular hydrogen bond $N3H^{+}$•••O5.

Keywords: FTIR spectroscopy, low-temperature matrix isolation, nucleosides, *ab initio* calculations.

Contents

1. Introduction

Investigation of the structure and physicochemical properties of biological molecules and their constituent fragments in an isolated state is of great interest for modern science [1–12]. This interest is due to a number of reasons, among which are usually distinguished: (i) the ability

to study the internal properties of biomolecules, unperturbed by the influence of surrounding molecules, (ii) the possibility of a detailed, step-by-step study of intermolecular interactions, (iii) the ability to use high-level quantum mechanical *ab initio* calculations for the interpretation of experimental data. At various stages of such studies, biomolecules are subjected to heating, cooling, intense laser irradiation, and ionization. The behavior of biological molecules under extreme conditions can be a source of useful information for fundamental astrophysical and astrochemical studies [13–15], as well as for the practical aspects of human expansion in space. Isolation of biomolecules from strong intermolecular interactions is achieved in a rarefied gas phase or in an environment of inert molecules that weakly interact with each other. In many cases, the most complete information about the structure of an isolated molecule is provided by vibrational spectra. However rotational broadening significantly complicates the analysis of the gas phase vibrational spectra even for simple molecules. The use of low temperatures can partially or completely solve this problem. For example, matrices of inert gases with weak van der Waals interactions insignificantly affect the internal properties of molecules but hinder their rotation. For example, tautomers of the DNA base cytosine were detected in the argon matrices [16, 17] using the classical method of low-temperature matrix isolation spectroscopy [18]. Low thermal stability of even simple biomolecules (amino acids, nucleic acid bases) limited their matrix isolation spectroscopic studies in the isolated state.

Nowadays, various methods of action spectroscopy are widely used to study isolated molecules. These methods use supersonic beams, tunable lasers, and mass spectrometers to obtain vibrational spectra [1–12, 19–22]. Due to their high sensitivity, these methods were used to study the spectral characteristics of a large number of neutral molecules (DNA and RNA fragments, amino acids, peptides, sugars), their ions and various complexes. There are many excellent reviews that describe in detail, main results in this area [1–12]. Therefore, in this work, we focus only on the results obtained by various low-temperature methods for such structural elements of DNA and RNA as nucleosides. A nucleoside is a compound molecule in which a nucleic acid base is linked by a glycosidic bond to a five-membered sugar ring of ribose (RNA) or deoxyribose (DNA) [23]. The nucleobase fragment or sugar ring of the nucleoside can be modified and, as a result, the conformational structure and biological functions of the nucleoside can be changed. Modified nucleosides are often used to create new drugs [23, 24], and therefore, the study of the structural features and properties of canonical nucleosides is of great interest. The glycosidic bond significantly reduces the thermal stability of nucleosides as compared to DNA/RNA bases. However, we were able to obtain FTIR spectra of pyrimidine nucleosides (uridine, thymidine) in inert matrices for the first time [25]. Moreover, to transfer these nucleosides to the gas phase, the thermodynamical equilibrium process of evaporation from the Knudsen cell was used. The complex, non-rigid conformational structure makes these molecules sensitive to the experimental conditions. Therefore it is of great interest to compare in this review the results obtained by different methods of absorption spectroscopy and action spectroscopy.

2. Experimental methods of low-temperature spectroscopy of nucleosides

2.1. Action spectroscopy

At room temperature, even simple biomolecules (DNA bases, amino acids) are in a solid phase. Since many biomolecules are destroyed at heating, the sensitivity of the research method and its additional capabilities for converting biomolecules into the gas phase are important. Therefore now for the study of the vibrational spectra of isolated molecules the most used methods of action spectroscopy. These methods change the populations of different molecular configurations in a molecular beam using tunable lasers. The high sensitivity of action spectroscopy is largely due to the mass spectrometric method of measuring the intensity of the molecular beam.

The infrared–ultraviolet (IR–UV) double resonance spectroscopy method is widely used to study molecules in a neutral form [1–6, 26]. The general scheme of the method is shown in Fig. 1. In most cases molecules (molecular weight up to 2000 Da) are injected into a supersonic inert gas beam using a pulsed laser (Fig. 1). A pulse from a scanning IR laser irradiates a supersonic beam by 100–400 ns earlier than a UV laser pulse which is pre-tuned to the main (intense) vibronic absorption band of a molecule in the ground state [26] and produces ions. The absorption of IR photons leads to a decrease in the population of the ground state and, respectively, to a decrease in the ion current in the mass spectrometer detector [26]. Therefore, this method is often called IR–UV ion dip spectroscopy [26]. A noticeable advantage of this method is the possibility of recording the IR spectra of individual conformers [26]. However IR–UV ion dip spectroscopy only works when a UV chromophore is present in the molecule under study.

The helium nanodroplet isolation (HENDI) spectroscopy method can be considered more versatile in relation to the structure of the molecule [20–22]. In this method, a supersonic beam is used to condense gaseous helium. The impurity of a molecule under study is incorporated directly into nanodroplets (nanomatrices) of liquid He which is in a superfluid state (T = 0.38 K). The intensity of the supersonic beam of He nanodroplets decreases when the frequency of the tunable IR laser coincides with the absorption frequency of the impurity molecule. Mass spectrometers and low-temperature bolometers are used to monitor the beam intensity [21, 22]. For example, in one of the HENDI spectroscopy implementations, impurity nanoclusters

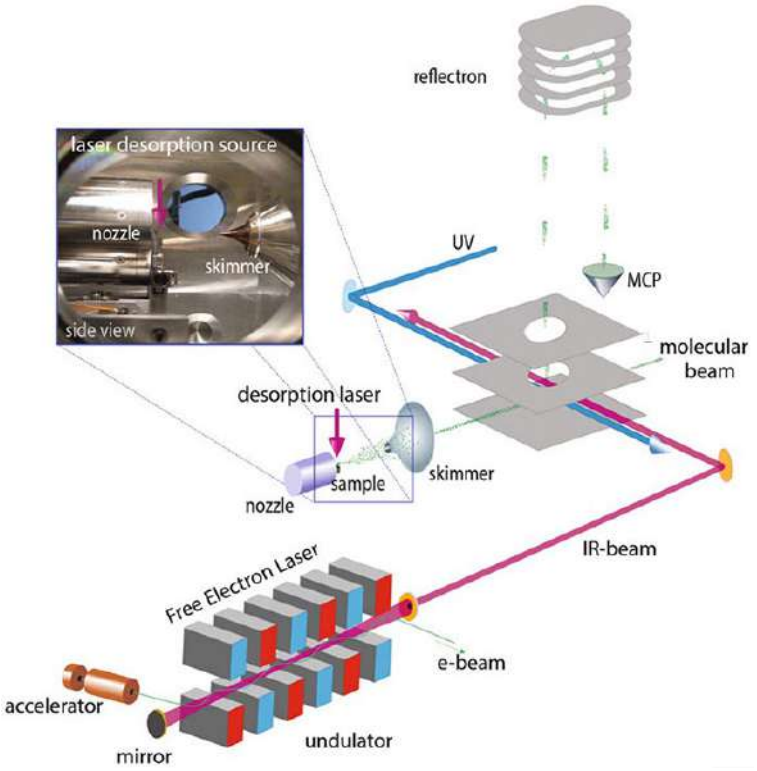

Fig. 1. (Color online) Scheme of the molecular beam setup equipped with a laser desorption source and a reflectron time-of-flight mass spectrometer used for IR–UV double resonance experiments at the free-electron laser facility (FELIX). The inset shows details of the laser desorption source [26].

were ionized by an electron beam and the beam intensity was monitored using a mass spectrometer [27, 28]. This method was the first to obtain the IR spectra of the simplest amino acid glycine in He nanodroplets [29]. It should be noted that in a similar way restrictions on the structure of the molecule in UV ion dip spectroscopy can be avoided by using non-selective ionization of the molecular beam by vacuum ultraviolet (VUV) irradiation [26].

Another method of the action spectroscopy of neutral molecules is now beginning to be applied. In this method, VUV ionization is also used [30, 31]. As shown in Fig. 2, the general scheme of this method is very similar to the UV ion dip spectroscopy (Fig. 1). But in this method a tunable pulsed IR laser is used for infrared multiple photon dissociation (IRMPD) of the molecule under study. Further to evaluate the degree of dissociation of molecules, one-photon ionization by a vacuum ultraviolet laser and signal registration by time-of-flight (TOF) mass spectrometer is used [30, 31].

The close integration of action spectroscopy with mass spectrometry has made it possible to apply a number of technical solutions from the field of mass spectrometry and obtain infrared absorption spectra of isolated molecular ions [19, 34]. For example, the combination of the processes of evaporation and ionization of molecules using electrospray (Fig. 3) has significantly increased the capabilities of the IRMPD method in studying large molecules [32, 33]. As a result the IRMPD spectra of various ionized DNA fragments were obtained [33].

The use of cryogenic ion traps and isolation of ions in He nanodroplets (Fig. 4) provides additional opportunities for the IRMPD method [32, 34]. Cooling the ions improves spectral resolution and expands the possibilities of studying complex molecular structures and their complexes. For example, the helium nanodroplet IR action spectroscopy

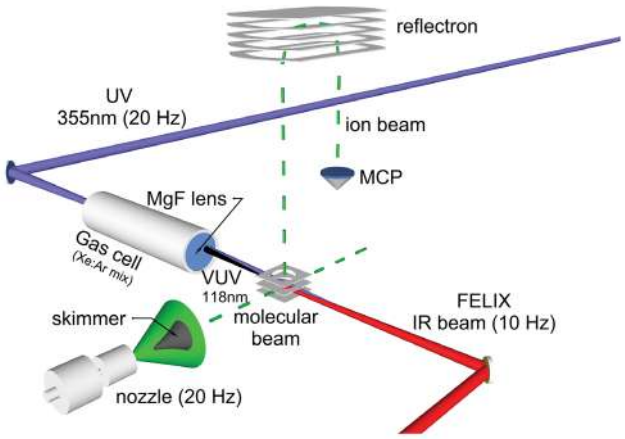

Fig. 2. (Color online) Scheme of the setup for the infrared (IR) action spectroscopy of low-temperature neutral gas-phase molecules. The IR photons were resonantly absorbed leading to infrared multiple photon dissociation (IRMPD). The IRMPD products were ionized with vacuum ultraviolet laser and the ionized species were analyzed with a time-of-flight reflectron-type mass spectrometer [30].

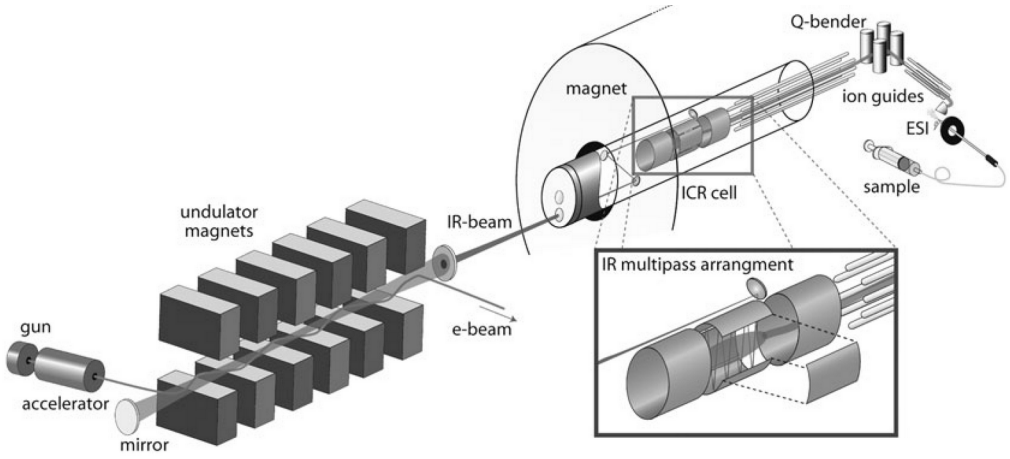

Fig. 3. Scheme of the setup with the Fourier-transform ion cyclotron resonance (FTICR) mass spectrometer, electrospray ionization (ESI), and source hexapole ion guide used for IRMPD ion spectroscopy at the FELIX facility [8].

method was used to obtain high-resolution spectra for a number of DNA dinucleotide anions within the helium nanodroplet [35]. The use of cryogenic ion traps made it possible to characterize the products of ion-molecular reactions and to study the structures of solvated clusters [36, 37].

2.2. Absorption spectroscopy

Despite the emergence of new methods, the absorption spectroscopy of isolated molecules remains a useful research tool and is enriched with new possibilities. In particular, a cavity ringdown spectroscopy which is a modern modification of gas-phase spectroscopy [38] should be noted. This method allows one to analyze such complex processes as the formation of intermolecular hydrogen bonds between DNA and RNA bases [39]. Significant improvements have also been made in the field of microwave spectroscopy [40]. This made allows one to obtain and analyze microwave spectra of many thermally unstable molecules including nucleosides [41].

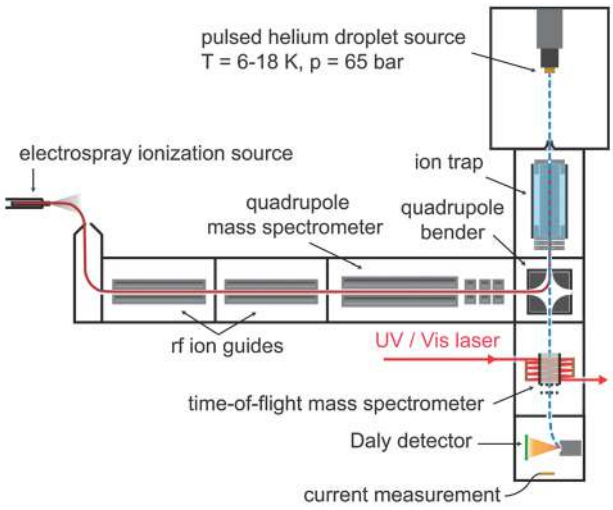

Fig. 4. (Color online) Scheme of the setup with helium droplet machine and ESI source for cold-ion spectroscopy, constructed at the Fritz Haber Institute by von Helden and coworkers [34].

Matrix isolation spectroscopy is another option for absorption spectroscopy and is widely used to study small biological molecules in an isolated state. Matrix isolation spectroscopy differs from most of the above methods by the possibility of long-term accumulation and preservation of the studied molecules in low-temperature inert matrices. The basic design of the cryogenic unit used for recording the FTIR spectra of matrix isolated nucleosides is shown in Fig. 5. The feature of this design is the low-temperature quartz microbalance (QCM) [42, 43] and the design of the evaporation unit [44, 45].

The QCM allows controlling the intensity of molecular flows of studied molecules and an inert gas. The cooled electrode of the QCM measuring quartz can be a mirror substrate for deposition of the matrix [43]. Most of the studied biomolecules are thermally unstable. Such molecules have a very low vapor pressure at temperatures below the thermal degradation threshold. Therefore we developed new design of the evaporator allowing accumulation

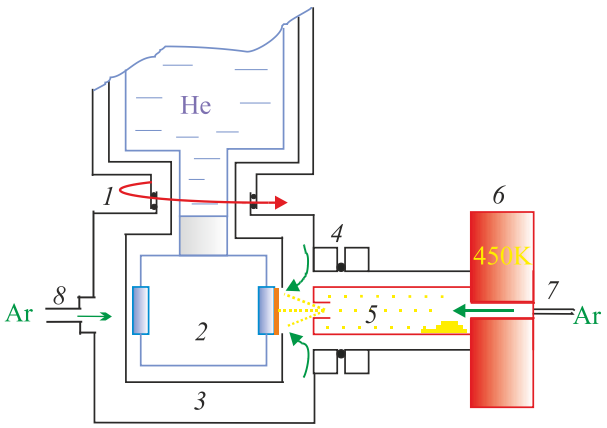

Fig. 5. (Color online) The general scheme of low-temperature setup based on liquid He cryostat: rotating vacuum seal (*1*), cryogenic block with cold mirrors and QCM (*2*), rotating nitrogen shield (*3*), flange with indium seal (*4*), Knudsen cell (*5*), an electric heater of Knudsen cell (*6*), Ar flow through Knudsen cell (*7*), outside Ar flow (*8*). Adapted from [44].

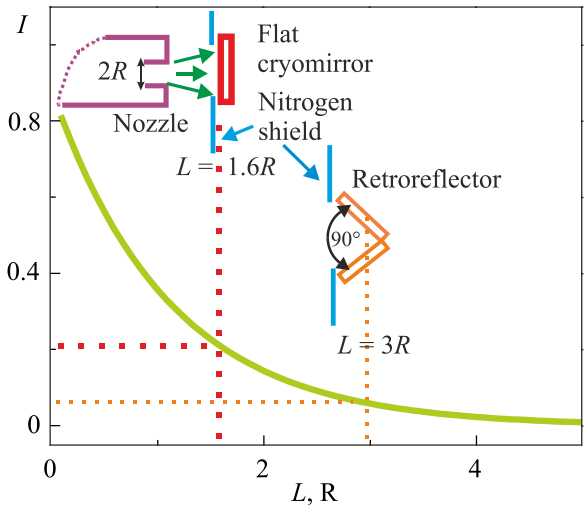

Fig. 6. (Color online) The evaporation scheme with flat cryomirror and cryoretroreflector with the relationship of the intensity of molecular beam I as function of the distances L between the cell and cold mirror. L is in the unit of radius R of the outlet nozzle of Knudsen cell. The dotted lines show the actual distances that were used in the experiments [46].

of a sufficient number of molecules in the sample in a reasonable time. The main idea of the design was to allow the maximum quantity of sublimated molecules to reach the matrix [44, 45].

The construction of this Knudsen cell is characterized by the working pressure less than 10^{-4} Torr and Knudsen number more than 100 [44]. For this cell, the dependence of the molecular beam intensity on the distance L to the cold mirror was obtained (Fig. 6) using the statistical Monte Carlo method [42]. In different experiments, the distance L was varied from $4.5R$ to $1.6R$ (Fig. 6) [25, 44–46]. Despite the small gap between the Knudsen cell and the cold mirror we were able to work even with Ne matrices at 5 K. Stable molecular flows with intensity of 40–60 ng/s·cm^2 were obtained using this design (Figs. 5 and 6) for thymidine, uridine [25] and glucose [25, 47] without their thermal decomposition.

2.3. Effect of cooling rate on interconversion of molecular configurations

Despite the technical differences, the methods discussed above have a common feature which is the need to cool the studied molecule to cryogenic temperatures in order to obtain spectra with good resolution. The cooling method is very important for non-rigid (labile) molecules since it may change the conformational equilibrium of the gas phase [48]. Even collisions of cold molecules may change the population of structures separating by low barriers [49]. Experiments with cooling molecules in supersonic beams show that the equilibrium does not change if the barrier between conformers exceeds 400–800 cm^{-1} [48–52]. When cooled in supersonic beams, the interconversion speed increases in the series of inert gases: He, Ar, Kr, and Xe [52]. The analysis of interconversion processes at the qualitative level can be performed on the basis of simplified kinetics of the transition through the energy barrier [46]. According to conventional transition state theory (TST) the classical rate constants K_{TST} may be estimated from the Eyring equation [53]:

$$K_{TST} = \frac{k_B T}{h} e^{-\Delta G^{\#}/RT}, \qquad (1)$$

where $\Delta G^{\#}$ is free energy of the barrier, h and k_B are Planck and Boltzmann constants.

Analogously to work of Jensen and Gordon for glycine [53], the Wigner correction of quantal tunneling effects was made as [46]:

$$K^{w}_{TST} = K_{TST}\left(1+\frac{1}{24}\left(\frac{h\nu}{k_B T}\right)^2\left(1+\frac{RT}{\Delta G^{\#}}\right)\right), \qquad (2)$$

where the imaginary frequency at the saddle point is denoted as ν.

Under the assumption that only forward transition will occur, the number of molecules dN which were passed through the barrier in a time dt may be expressed as [46]:

$$dN = -K^{w}_{TST} N dt\ . \qquad (3)$$

Table 1. The $T_{1/2}$ time (s) of transition of one-half number of molecules from the one conformer to another calculated by Eqs. (1)–(5) (the reverse transition was ignored) [46]

Barrier, kcal/mol	The $T_{1/2}$ time (s) for different T (K)				
	430 K	300 K	200 K	12 K	6 K
0.3	$1.1\cdot10^{-13}$	$1.9\cdot10^{-13}$	$3.7\cdot10^{-13}$	$1.2\cdot10^{-6}$	9.0
0.7	$1.7\cdot10^{-13}$	$3.5\cdot10^{-13}$	10^{-12}	9.9	$2.5\cdot10^{13}$
1.3	$3.4\cdot10^{-13}$	10^{-12}	$4.6\cdot10^{-12}$	$8\cdot10^{11}$	$> 2.5\cdot10^{13}$
2.0	$8\cdot10^{-13}$	$3\cdot10^{-12}$	$2.5\cdot10^{-11}$	$> 8\cdot10^{11}$	$> 2.5\cdot10^{13}$
3.0	$2.6\cdot10^{-12}$	$1.7\cdot10^{-11}$	$3\cdot10^{-10}$	$> 8\cdot10^{11}$	$> 2.5\cdot10^{13}$

Integration of Eq. (3) with the initial number of molecules N_0 leads to

$$N(t) = N_0 e^{-K_{TST}^w t}. \quad (4)$$

It follows that time $T_{1/2}$ of the transition of one-half number of molecules from the one conformer to another may be expressed as [46]:

$$T_{1/2} = \frac{\ln 2}{K_{TST}^w} = \frac{0.693}{K_{TST}^w}. \quad (5)$$

Obviously, depopulation of the low-barrier conformers (conformational cooling [46, 52]) will occur if the time of energy relaxation is close to $T_{1/2}$. The results of calculations using Eqs. (1)–(5) for the different temperatures and height of barriers are summarized in Table 1 [46].

As it is seen from Table 1 and extrapolation of the experimental data [54, 55], the conformers with the barrier about 0.7 kcal/mol may be easily conserved in the isolated state at the temperature of 6 K. But it is possible only under the condition that the process of relaxation energy is very fast, otherwise the population of conformers will be changed. Obviously, the cooling rates will differ for different methods of cooling the impurity molecules. The cooling will be the slowest when the impurity molecules are introduced into the subsonic zone of a supersonic beam. It can be assumed that the widely used scheme of introducing molecules into the beam in front of the skimmer (Fig. 1) [26] is also not optimal. The reason is collisions of molecules in the "hot" shell of the supersonic beam before they reach its cold core.

The more rapid energy relaxation and consequently effective "conformational quenching" may happen at the "pick-up" cell [21, 22, 28] with direct contact of impurity molecules and superfluid helium nanodroplets in HENDI spectroscopy or at the surface of the low-temperature matrices. Poliakoff and Turner [56] noted what the rate of relaxation energy is subject to variation directly as frequencies of the phonon spectrum. It is known, that the frequencies of the phonon spectra increase in the row of matrices: Xe, Kr, Ar [57]. Some experimental results of matrix isolation spectroscopy are in good agreement with this hypothesis [54]. It is interesting that the frequency of the phonon spectrum of Ne cryocrystals has the middle position between Kr and Ar [57].

3. Quantum mechanical calculations of the conformational structure of nucleosides

Nucleosides are the main building blocks of DNA and RNA. Natural canonical nucleosides include guanosine, adenosine, cytidine, and thymidine (uridine in RNA) [23]. Nucleosides have a flexible, non-rigid structure. As it was shown for thymidine and adenosine, the structure of nucleosides is mainly determined by four intramolecular rotations and by the non-rigid structure of the sugar ring (Figs. 7 and 8).

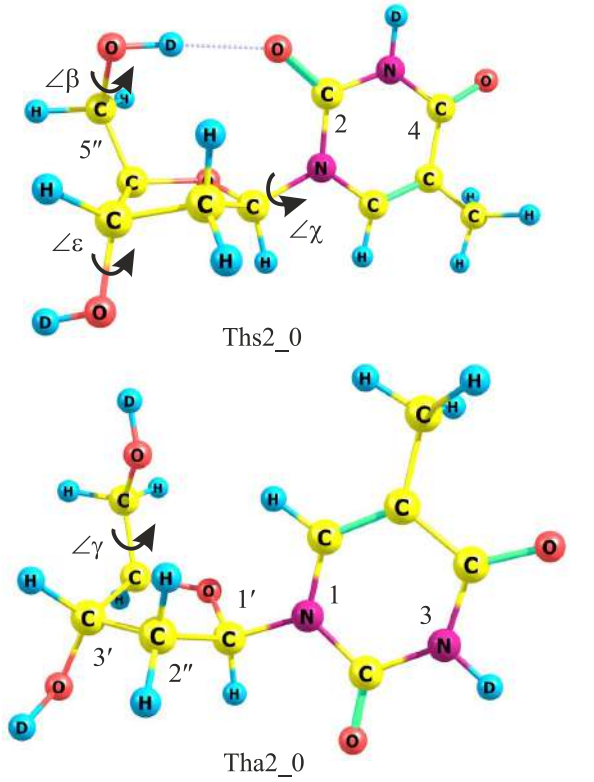

Fig. 7. (Color online) Atomic numbering, torsion angles, and molecular structures of the main *syn*- (Ths2_0) and *anti*- (Tha2_0) conformational isomers of thymidine. The dotted line shows the intramolecular hydrogen bonds.

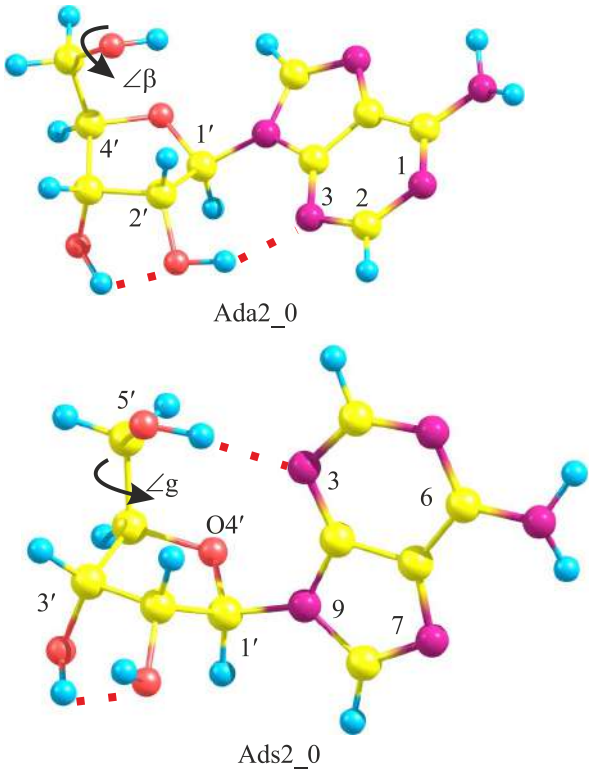

Fig. 8. (Color online) Atomic numbering, torsion angles, and molecular structures of the main *syn*- (Ads2_0) and *anti*- (Ada2_0) conformational isomers of adenosine. The dotted line shows the intramolecular hydrogen bonds.

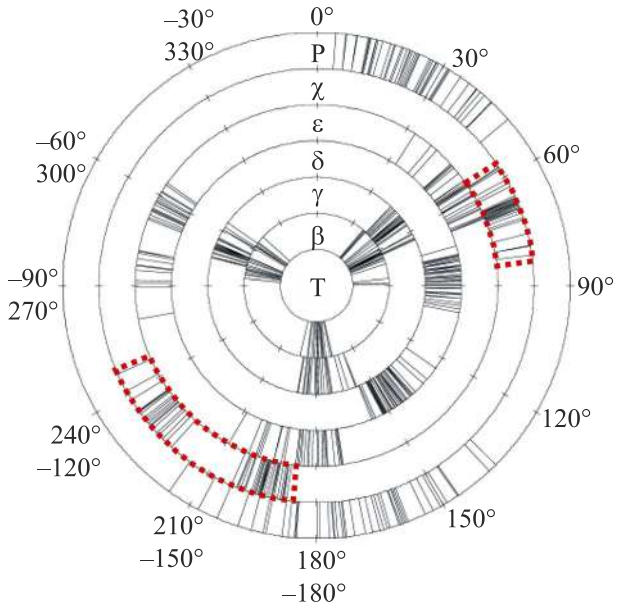

Fig. 9. Pie chart of the distribution of the all Th conformers over torsion angles. The dotted lines show the areas of *syn*-conformers ($55° < \chi < 85°$) and *anti*-conformers ($190° < \chi < 250°$) [66].

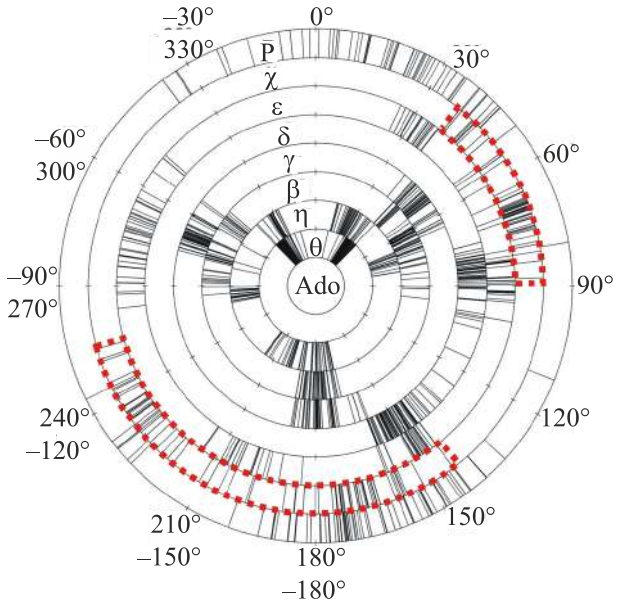

Fig. 10. Pie chart of the distribution of the all Ad conformers over torsion angles. The dotted lines show the areas of *syn*-conformers ($40° < \chi < 88°$) and *anti*-conformers ($140° < \chi < 250°$) [69].

Structural investigations of highly flexible nucleoside molecules are impossible without performing of modern quantum mechanical calculations. Earlier the quantum mechanical calculations were used to study only certain structural and spectral properties associated with the limited experimental information [58–63] since the vibrational spectra of isolated nucleosides were not available. New experimental spectral data obtained for isolated nucleosides has stimulated a detailed study of their conformational space.

Conformational space of a nucleoside molecule may be described using several dihedral angles: O4′C1′N1C2 for pyrimidine nucleosides and O4′C1′N9C4 for purine nucleosides ($\angle\chi$), C3′C4′O5′H ($\angle\beta$), C2′C3′C4′O5′ ($\angle\gamma$), C4′C3′O3′H′ ($\angle\varepsilon$) [23]. Structure of ribose or deoxyribose residues usually may be described by a pseudo rotation angle: ($\angle$P) [23, 64] but additional dihedral angles may be also used: C5′C4′C3′O3 ($\angle\delta$), C3′C2′O2′H ($\angle\eta$), and O3′C3′C2′O2′ ($\angle\theta$).

For the conformational analysis of the structure of nucleosides, the “brute-force” method turned out to be the most effective. It consists in sequential scanning of dihedral angles. This is due to the relatively small number of dihedral angles describing the structure of nucleosides. The most detailed search for stable conformations of canonical nucleosides and some of their derivatives was carried out by Zhurakivsky *et al*. [65–72]. For example, 92 stable conformers of thymidine [65] and 103 conformers of adenosine [69] were located in the calculations performed at the of DFT/B3LYP/6-31G(d,p) level of theory. The examples of resulting distributions of the torsion angles of the nucleoside conformers are shown in Figs. 9 and 10 for thymidine and adenosine, respectively.

It is clear what all predicted nucleoside conformers cannot be observed in experiment even if very sensitive methods are applied. First of all this is due to high relative energies of the most calculated conformers. The detection threshold of 2.5 kcal/mol with respect of the lowest energy conformers reduces the number of potentially observable conformers to 8 for adenosine and 29 for thymidine. Moreover the possible conformer interconversion during matrix deposition should be taken into account. Therefore in the calculations associated with the analysis of the experimental spectra obtained by the matrix isolation method much attention was paid to the analysis of the height of the energy barriers separating the nucleoside conformers.

Quantum chemical calculations of the nucleosides were performed using the program packages Gaussian 09 [73] and Firefly (version 8.0) [74]. The later partially uses the GAMESS (US) program code [75]. In most investigations, the geometry optimization was performed using the second-order many-body perturbation theory (MP2) and density functional theory (DFT/B3LYP [76]) methods. As a rule, standard basis sets, such as cc-pVDZ [77] or 6-311++G(df,pd) were used in the calculations. In this review, conformations with *anti*- and *syn*-structures of the ribose (deoxyribose) ring are denoted as Yan_x and Ysn_x, respectively, where Y designates certain nucleoside (for example, Th — thymidine, 2dU — 2deoxyuridine, Ad — adenosine ets.), n designates conformation of the sugar ring (2-C2′-endo or 3-C3′-endo) and x correspond to the conformer numbers in order of increasing their relative energy. The DFT/B3LYP method was used in combination with the empirical dispersion correction (D3 or D3(BJ) [78, 79]) to improve the accuracy of calculating energies. As we demonstrated earlier, the use of the D3

or D3(BJ) corrections improves the agreement between calculated and experimental frequencies of the νOH, νNH stretching vibrations of nucleosides [80]. Also the polynomial correction method [81] may be helpful to further reduce the difference between calculated and experimental frequencies.

4. Vibrational spectra and structure of pyrimidine nucleosides at low temperatures

4.1. 2-deoxyuridine and thymidine in Ar *matrices*

IR spectra of thymidine (Th) and uridine (Ur) in argon matrices were obtained in 1998 [25] for the first time. In this work [25] the possibility of long-term sublimation of nucleosides was demonstrated. More sophisticated analysis of the experimental spectra and conformational equilibrium was carried out in subsequent works for Th, Ur, and the minor nucleoside 2-deoxyuridine (2dU) [44–46, 82–84].

The region of stretching vibrations of Th and 2dU isolated in Ar matrices is shown in Fig. 11. This figure also shows the FTIR spectra of 1-methylthymine and thymine. The spectrum of 1-methylthymine allowed exact identification of the νN3H vibration of Th and 2dU molecules (Fig. 11). Comparison of the spectra of nucleosides and bases (thymine, 1-methylthymine) showed that characteristic very narrow bands of bases are absent in the spectra of nucleosides. This indicates that, upon evaporation of nucleosides, the cleavage of the glycosidic bond between the pyrimidine and ribose fragments of the nucleoside does not occur. This is reliable evidence that thermal destruction of Th and 2dU did not occur during evaporation of the nucleosides in the temperature range of 415–435 K [44–46, 82, 83]. In mass spectrometric experiments the thermal stability threshold of nucleosides is noticeably lower. For example, a temperature stability threshold of 420 K was found in experiments with electron impact ionization of thymidine [85]. The destruction of Th under VUV ionization began at 410 K [86].

Rotation around the glycosidic bond (angle χ) divides the conformational space of a nucleoside into *anti*- and *syn*-subspaces [23]. Calculations estimate the height of the barrier between these subspaces to be more than 4 kcal/mol for 2dU [82] and more than 6 kcal/mol for Th [83] (Fig. 12). Annealing the matrices at 30 K showed no significant changes in the spectra and confirmed the existence of a high barrier between the *anti*- and *syn*-subspaces [83]. This allows us to assert that interconversion between the *anti*- and *syn*-conformers did not occur in low-temperature inert matrices. At the same time, rotation of small nucleoside fragments corresponding to dihedral angles ∠β, ∠γ and ∠ε are possible within the subspaces. Pseudo rotation of the ribose ring (dihedral ∠P) is also possible. This increases probability of the nucleoside conformer interconversion and requires a detailed analysis of the height of the energy barriers between individual conformers. An analysis of experimental results and calculations showed that the minimum barrier height that allows fixing nucleoside conformers in Ar or Kr matrices can be estimated as 2 kcal/mol [83]. All main conformers of 2dU and Th fixed in matrices were identified. Their population in the gas phase at the evaporation temperature [82, 83] was calculated. Based on experimental integral intensities of the characteristic spectral bands of individual conformers we estimated their populations in Ar matrices [83]. As shown in Fig. 13, only 5 Th conformers make a significant contribution to the experimental FTIR spectrum.

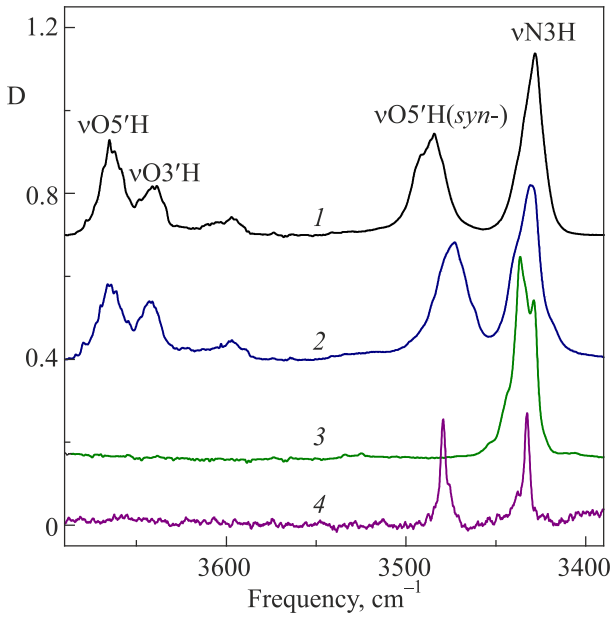

Fig. 11. The region of νOH, νNH stretching vibration of thymidine conformers (*2*), as well as 2′-deoxyuridine (*1*), 1-CH3-thymine (*3*), and thymine (*4*) in an Ar matrix [83].

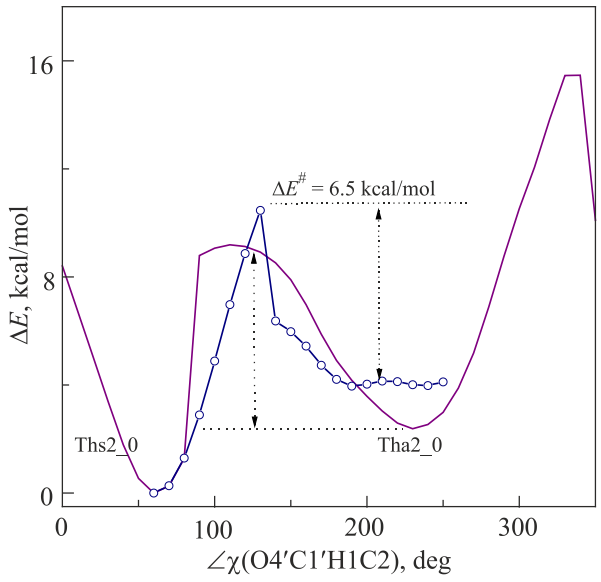

Fig. 12. The profile of the barrier of the *anti* → *syn*-conformational transition in isolated thymidine calculated by the DFT//B3LYP//cc-pvdz method with a step of 10° along the torsion angle χ. The circles indicate the profile of motion from *syn* (Ths2_0) to *anti* (Tha2_0) [83].

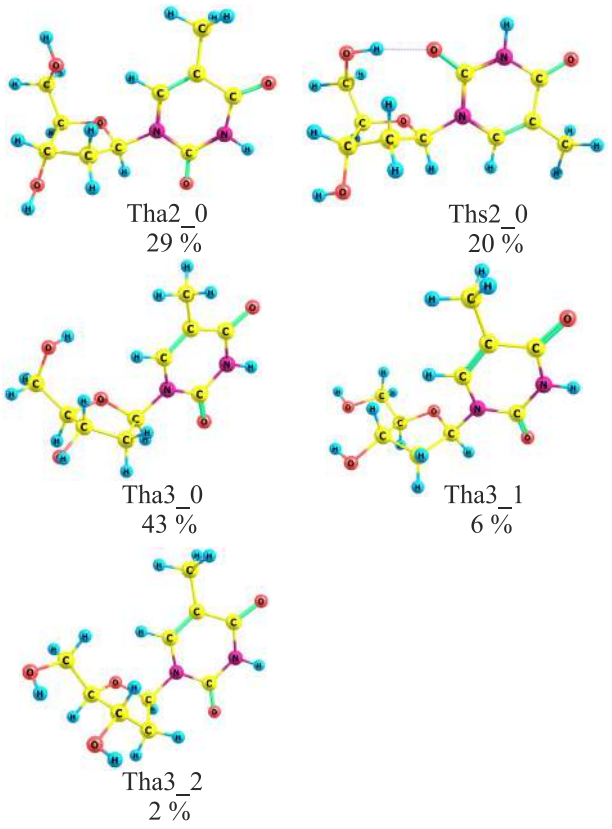

Fig. 13. (Color online) The conformers of thymidine that are fixed in the matrix and estimation of their population (%) in Ar matrices [83].

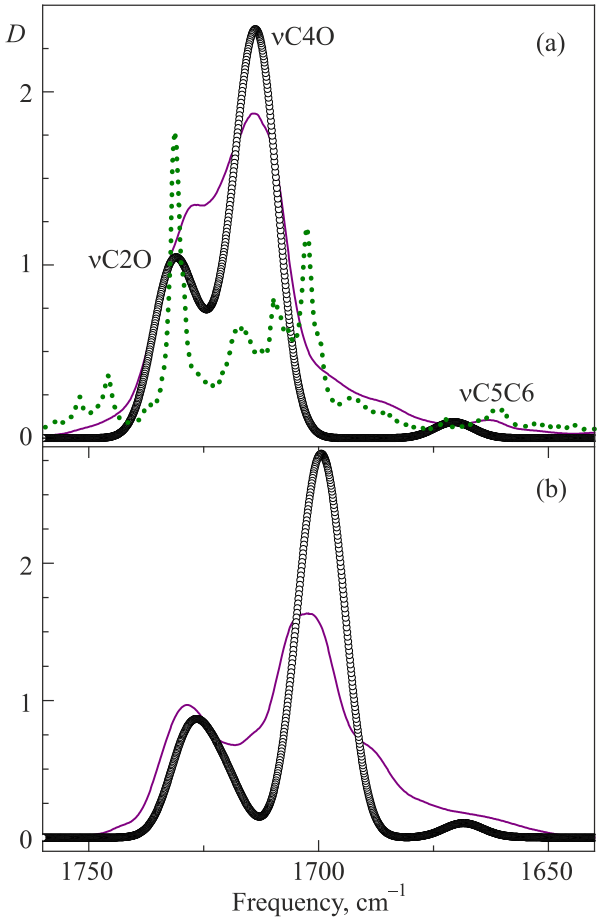

Fig. 14. The region of stretching vibrations of the CO group (νCO) for thymidine, 1-methylthymine (a) and trideuterothymidine (b) in Ar matrices. The spectrum of 1-methylthymine is shown by a dotted line. The line composed of circles shows a visualization of the calculated spectra of nucleosides [83].

Analyzing the experimental spectra of nucleosides it is also necessary to take into account the splitting of the spectral bands caused by the Fermi resonance. The Fermi resonance is especially often manifested in the region of the absorption bands of CO stretching vibrations of pyrimidine bases [40]. For example, 5 additional absorption bands appear in this region in the FTIR spectrum of 1-methylthymine [Fig. 14(a)].

Comparison of the experimental and calculated (synthesized with accounting for the conformer populations (Fig. 13) spectra of Th demonstrated a significant overlap of the νC2O and νC4O spectral bands [Fig. 14(a)]. Such a broadening of the absorption bands of νCO vibrations can also be caused by the Fermi resonance.

The possibility of the manifestation of the Fermi resonance in this spectral region was also indicated by the results of calculations by the VPT2 method which takes into account the anharmonicity of vibrations [83]. According to these calculations, Fermi resonance between CO stretching vibrations and several combination modes is possible. Deuteration of Th changed the resonance conditions significantly. As a result, in the experimental spectrum of deuterated Th one can see a clear separation of the absorption bands of the νC2O and νC4O vibrations and good agreement between the experimental and calculated spectra was observed [Fig. 14(b)].

Absorption bands of the νOD and νND vibrations were shifted to the region of 2700–2500 cm^{-1} in the spectrum of deuterated Th and their intensities were decreased significantly [Fig. 15(b)]. The results of calculations of vibrational spectra by the DFT/B3LYP/6-311++G(df,pd) method in the harmonic approximation and with a scaling factor of 0.96434 agree well with the experimental spectrum. This was observed for all spectral bands in this range, except for the νN3D vibration band. This band overlapped with the νO5′D band of the Ths2_0 conformer and is split into two bands with frequencies of 2552 cm^{-1} and 2533 cm^{-1}. The frequencies of these two bands are shifted in opposite directions from the calculated frequency of 2543 cm^{-1} (νN3D). The reason for this splitting is the Fermi resonance. This is facilitated by the fact that the band of νN3D vibration is shifted to the region of 2500–2800 cm^{-1} where several combination bands are located [87]. Earlier we detected the splitting of the νN3D vibration band caused by the Fermi resonance for deuterated 5I-uracil [87].

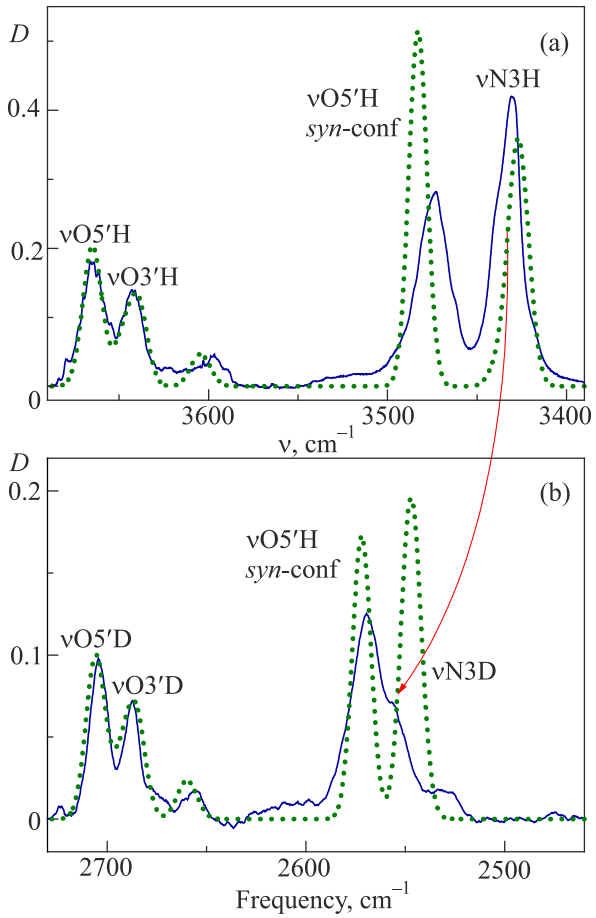

Fig. 15. The region of stretching vibrations (νNH, νOH) of thymidine (a) and (νND, νOD) of deuterothymidine (b) in Ar matrices. The dotted line shows a visualization of the calculated spectrum [83].

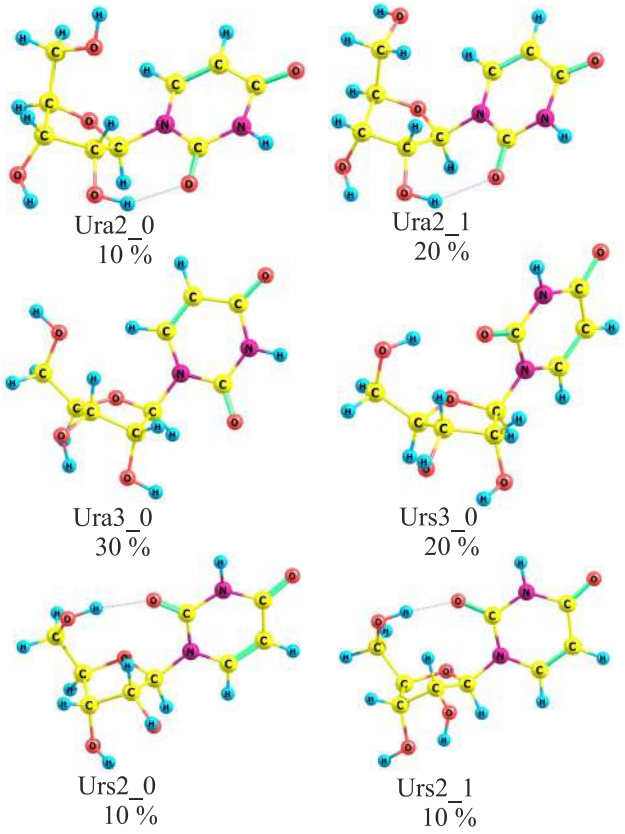

Fig. 16. (Color online) The conformers of uridine are fixed in the matrix and estimation of their population (%) in Ar matrices [84].

4.2. Uridine in Ar *matrices*

Compared to 2dU, the Ur molecule contains an additional hydroxyl group O2′H. As a result, intramolecular hydrogen bonds O2′H•••O2, O3′H•••O2′, and O2′H•••O3′ are formed in the various uridine conformers (Fig. 16). Matrix isolation FTIR spectroscopy and quantum-chemical calculations demonstrated that in argon matrices at 10–12 K most conformers (70 ± 10) % contain intramolecular hydrogen bonds formed by the carbonyl group (C2=O) (Fig. 16) [84]. FTIR spectra of Ur demonstrated an increase by (40 ± 10) % of the population of *syn*-conformers with the O5′H•••O2 intramolecular hydrogen bond [84] as compared to the spectra of 2dU. It is explained by the appearance in the matrices of the Urs3_0 conformer with the C3′-endo structure of the ribose ring. This result was supported by the calculation [84] of the energy relaxation profiles of the conformational transitions for the different pair conformers (Fig. 17). In this work [84], the population of conformers in the matrices was estimated using information about the experimental integral intensities of characteristic absorption bands of individual conformers. It was further confirmed by a comparison of the experimental spectrum and the calculated spectrum using Gaussian contours with half-width of 10 cm^{-1}. The calculated spectrum was produced as a sum of calculated spectra of individual Ur conformers with accounting for the conformer populations. It was done for both experimental and calculated populations. If we used the calculated populations of conformers the total calculated spectrum (Fig. 18, curve *3*) was found to be significantly different from the experimental spectrum (Fig. 18, curve *1*). However, using of experimental population (Fig. 16) resulted in a good agreement between the calculated and experimental spectra. (Fig. 18, curve *2*).

4.3. Uridine and protonated uridine in the gas phase

Structure of the gas phase uridine was studied by microwave spectroscopy method using broadband chirped pulse FT microwave spectrometer [41]. A laser ablation vaporization system was used to convert uridine to the gas phase. Rotational transitions of uridine were distinguished in the experimental spectrum (Fig. 19) despite the strong photo-fragmentation of uridine during laser ablation. Comparison of the experimental data with the results of calculations performed at the MP2-6-311++G(d,p) level of theory allowed authors to assign observed bands to the *anti*/C2′-endo-g+ conformer. Structure of this conformer

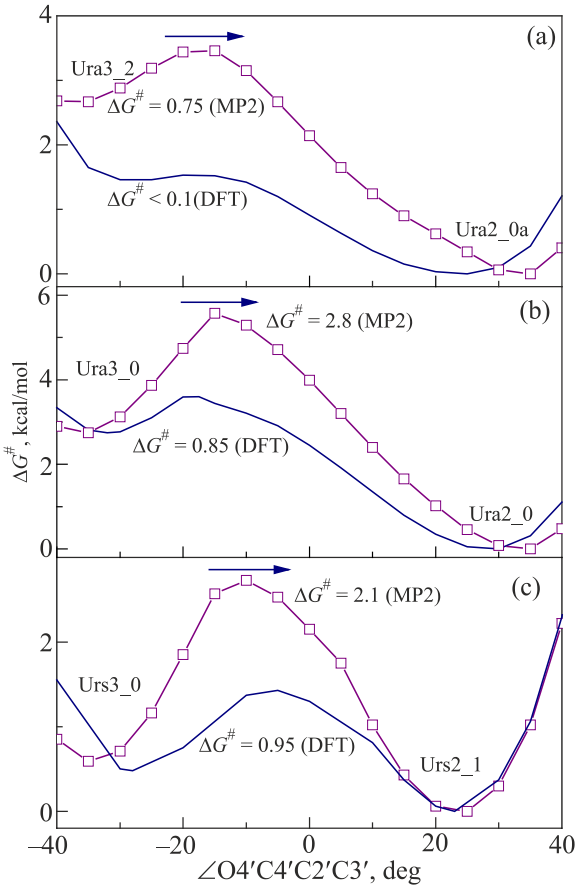

Fig. 17. The energy relaxation profiles of the conformational transitions for the different pair of *anti*- (a), (b) and *syn*-conformers (c) calculated by the DFT/B3LYP/cc-pVDZ and MP2//cc-pVDZ methods (squares) along dihedral angle O4′C4′C2′C3′ with the step of 10° [84].

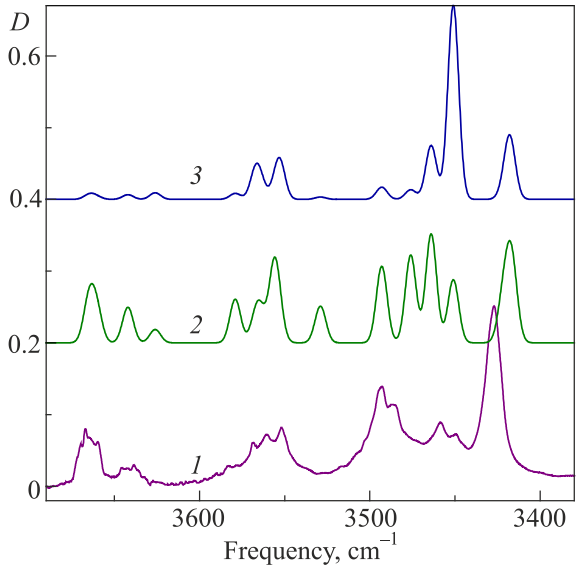

Fig. 18. The comparison of the experimental spectrum and the calculated spectra. The experimental spectrum of Ur isolated in Ar matrix (*1*); visualization of the calculated spectrum according the experimental estimation of the occupancies of the Ur conformers (*2*); visualization of the calculated spectrum according the computational estimation of the occupancies of the Ur conformers [84] (*3*).

is similar to the conformer Ura2_0 (Fig. 16) from the *anti*-conformational subspace which was detected in argon matrices earlier [84].

Many pyrimidine nucleosides were investigated in protonated form by action spectroscopy (IRMPD) [88–95]. Electrospray method is widely used in the study of ions. It combines the transfer of molecules into the gas phase and the ionization process.

The conformational landscape of protonated nucleosides changes significantly. These changes can be caused not only by the addition of a proton. It has been shown that tautomeric transitions can occur in molecules (for example, in uracil, thymine, and their nucleosides) in a protic solvent prior to (or during) their transfer into the gas phase by means of the electrospray process [94, 95]. Solvent molecules may act as a bridge that lowers the activation energy of tautomerization [94]. It was shown that 2,4-dihydroxy tautomers are dominant for the derivatives protonated forms of Ur and Th. O2-protonated tautomers represent the main group of minor Th and 5-methyluridine conformers [88, 89]. At the same time, atom O4 is protonated in the minor group of conformers (Fig. 20) in the case of $[2dU+H]^+$ and $[Ur+H]^+$ [88]. The number of conformers that are energetically favorable and can be detected in experiments is very small for each tautomeric group [88]. For example, only three conformers have populations sufficient for experimental detection (Fig. 20) within tautomeric subspace $[Ur+H]^+$. It should also be noted that calculated relative stabilities of protonated structures (Fig. 20) are highly dependent on computational method applied.

5. Vibrational spectra and structure of purine nucleosides at low temperatures

5.1. Guanosine and adenosine in the gas phase

In contrast to the pyrimidine nucleosides discussed above, the vibrational spectra of isolated purine nucleosides (2′-deoxyguanosine, 3′-deoxyguanosine, guanosine) were first obtained by action spectroscopy using the IR-UV ion dip or REMPI methods [96–100]. As shown in Fig. 21, spectra of guanosine and its derivatives under the conditions of these experiments were obtained only for the enol tautomers [97]. The conditions of resonant photoionization were apparently not optimal for the diketotautomer [96]. It is also interesting to note, that only one structure of guanosine was detected in supersonic beams: a *syn*-conformer with strong intramolecular hydrogen bond formed between 5′O-H group of ribose residue and 3-N atom of enol tautomer of guanine residue [96–100]. Taking into account the results obtained for the gas phase Ur (Fig. 19) [41], we can assume that the depletion of the conformational landscape in these experi-

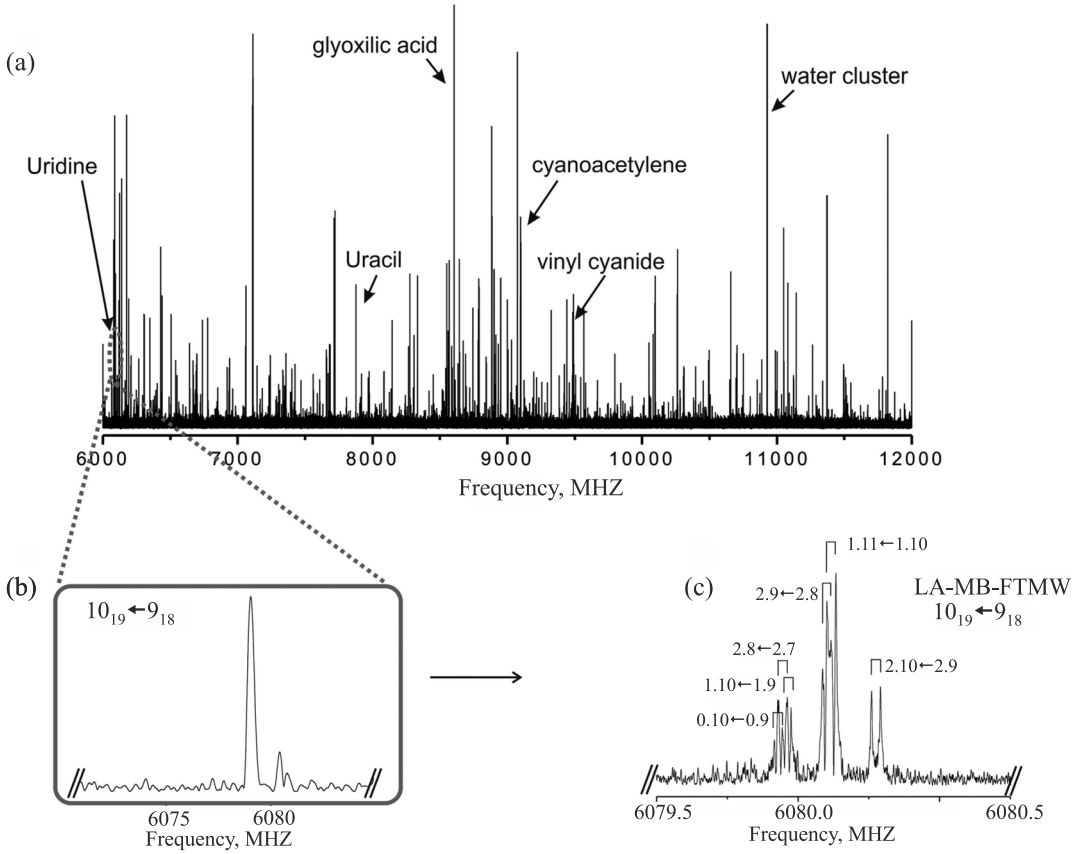

Fig. 19. (a) Spectrum of uridine in the frequency 6–12 GHz frequency region with some of the photofragmentation lines (b). A part of the broadband spectrum showing a not resolved $10_{19}\leftarrow9_{18}$ transition of uridine. (c) The $10_{19}\leftarrow9_{18}$ rotational transition of uridine showing its hyperfine structure completely resolved by FT microwave spectrometer [41].

ments may be explained by specific conditions of laser ablation and resonant photoionization.

Unlike guanosine, adenosine was found to be unstable to the specific conditions of the REMPI experiment [101]. However, IR–UV ion dip spectra of adenine and 9-methyladenine have been successfully obtained [101, 102]. The fragmentation of adenosine during laser vaporization may be caused not only by its instability. It has been suggested that adenosine has an efficient excited-state deactivation mechanism and exhibits a significantly shorter excited-state lifetime than adenine [103].

5.2. 2-deoxyadenosine and adenosine in Ar *matrices*

In the matrix-isolation experiments, 2-deoxyadenosine (2dA) and adenosine (Ad) were evaporated from Knudsen cell. Evaporation temperatures were 440 K for 2dA and 465 K for Ad [80, 104]. These temperatures are noticeably higher than in experiments with pyrimidine nucleosides. However, they are significantly lower than the known melting points of 2dA and Ad [105]. For example, the melting point of Ad is 510 K [105]. Therefore, we can say that the evaporation of 2dA and Ad took place in the sublimation mode. Similarly to the analysis of the Th and 2dU spectra (Fig. 11) in the region of stretching vibrations, a comparison was made between the spectra of the nucleoside and the adenine base. FTIR spectrum of adenine was also registered to simplify analysis of the nucleosides spectra in the fingerprint region.

Registered FTIR spectra are shown in Fig. 22. As it is seen, narrow spectral bands were absent in the spectrum of adenosine. These narrow bans are spectral markers of adenine. Therefore it demonstrated sufficient thermal stability of 2dA and Ad during prolonged sublimation in vacuum [80, 104]. It should be noted that similar evaporation of guanosine was not possible.

2dA in the gas phase and in low-temperature matrices was represented mainly by *syn*-conformers (Fig. 23) what makes it different from 2-deoxy pyrimidine nucleosides. In the matrices, the subset of *syn*-conformers of 2dA was represented by two conformers with the C2′-endo structure of the deoxyribose ring. The difference between these conformers was only in the rotation of the O3′H group (Fig. 23). In contrast to pyrimidine 2'-deoxy nucleosides, the matrices did not contain 2dA conformers with intramolecular O3′H•••O5′ and O5'H•••O3′ hydrogen bonds. It explains the absence of absorption bands of 2dA conformers in their FTIR spectra near 3600 cm^{-1} (Fig. 24). Frequency of the O5′H stretching vibration is strongly downshifted due to the intramolecular hydrogen bond O5'H•••N3 in *syn*-conformers (Fig. 24). UV irradiation of the matrix samples

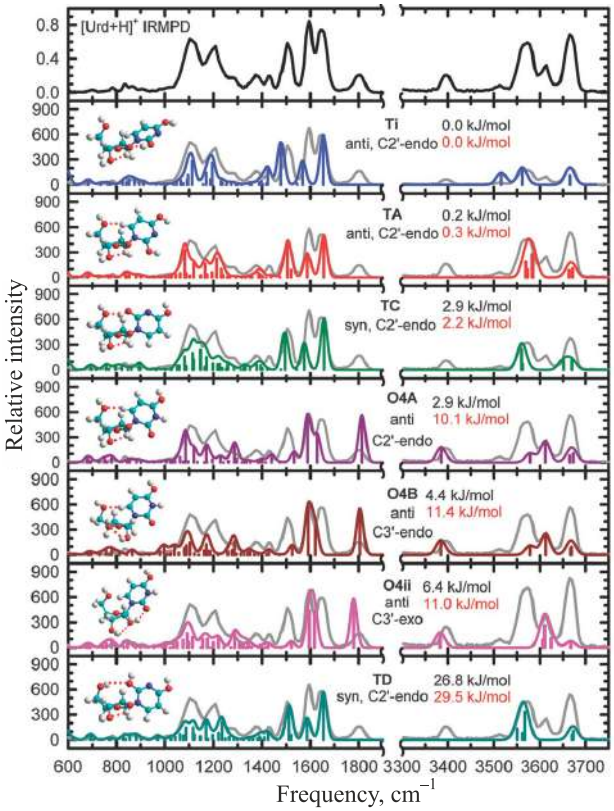

Fig. 20. (Color online) Comparison of the measured IRMPD action spectrum of $[Ur+H]^+$ with the calculated IR spectra for the low-energy conformers of $[Ur+H]^+$ that may be populated in the experiments and the corresponding structures calculated at the B3LYP/6-311+G(d,p) level of theory. Also shown in black are the B3LYP/6-311+G(2d,2p) and in red the MP2(full)/6-311+G(2d,2p) relative Gibbs free energies at 298 K [88].

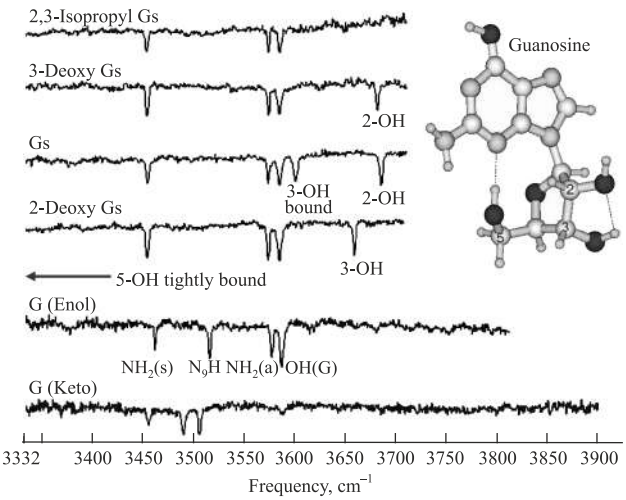

Fig. 21. The IR–UV ion dip spectra of laser-desorbed guanosine (Gs), 2-deoxyuanosine (2-deoxyGs) and 3-deoxyguanosine (3-deoxyGs) molecules. The IR spectra of 2,3-isopropylGs and G(enol, keto) are shown also. The inset shows the most stable guanosine structure at the HF/6-31G(d,p) level that is in agreement with the observed spectral bands [97].

leads to decrease of population of the *syn*-conformers. Characteristic bands of conformations with the C3′-endo structure of the deoxyribose ring were not found in the matrix FTIR spectra of 2dA [80].

The presence of the O2'H group significantly enriches the conformational landscape of the gas phase of adenosine (Fig. 25) [104]. It was shown that the population of the *anti*-conformers of Ad increased significantly as compared to dA due to the intramolecular hydrogen bond O2′H•••N3. At evaporation temperature of 465 K, the population of these conformers was more than 50 % higher than the population of *syn*-conformers with the O′H•••N3 hydrogen bond. Subsets of *syn*- and *anti*-conformers with the C2′-endo structure of the deoxyribose ring were detected in argon matrices at 6 K. Similarly to the 2dA FTIR spectra, absorption bands of Ad conformers with intramolecular hydrogen bonds O3′H•••O5′ or O5′H•••O3′ are not observed (Fig. 26). However, there are absorption bands of hydrogen-bonded groups O3′H and O2′H near 3590 cm^{-1} (Fig. 26). The frequency position of these bands is determined by the intramolecular hydrogen bonds O3′H•••O2′ and O2′H•••O3′. The absorption band of O2′H and O5′H groups of Ad was observed near 3270 cm^{-1} (Fig. 26). This bands is broad and intense due to the strong intramolecular hydrogen bonds O2′H•••N3 and O5′H•••N3. It should be noted that the absorption bands of the O3'H and O2'H groups of *syn*-conformations, have highest frequencies. In these conformations the oxygen atoms are proton acceptors in intramolecular hydrogen bonds O3′H•••O2′ or O2′H•••O3′ (Figs. 25 and 26). Unlike 2dA, the *syn*-conformers of Ad with the C3′-endo structure may be fixed in Ar matrices [104].

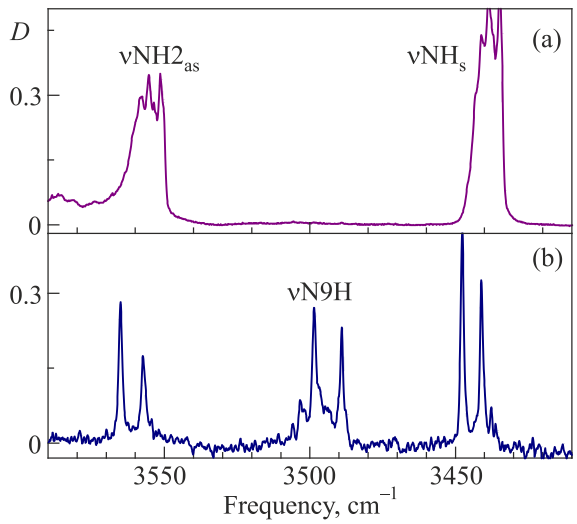

Fig. 22. Comparison of the vibrational spectra of adenosine (Ado) and adenine in the region of stretching vibrations νNH: (a) Ado in an Ar matrix (T = 8 K, M/S = 700); (b) adenine in Ar matrix (T = 12 K, M/S = 800) [104].

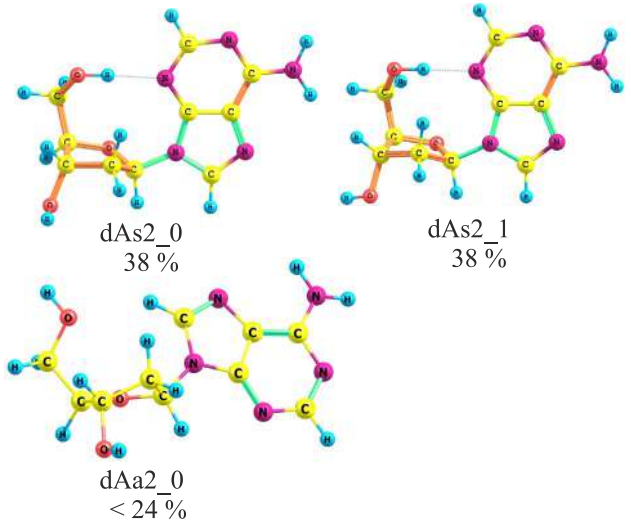

Fig. 23. (Color online) The conformers of dA that are fixed in the matrix and estimation of their population (%) in the Ar matrices at $T = 6$ K [80].

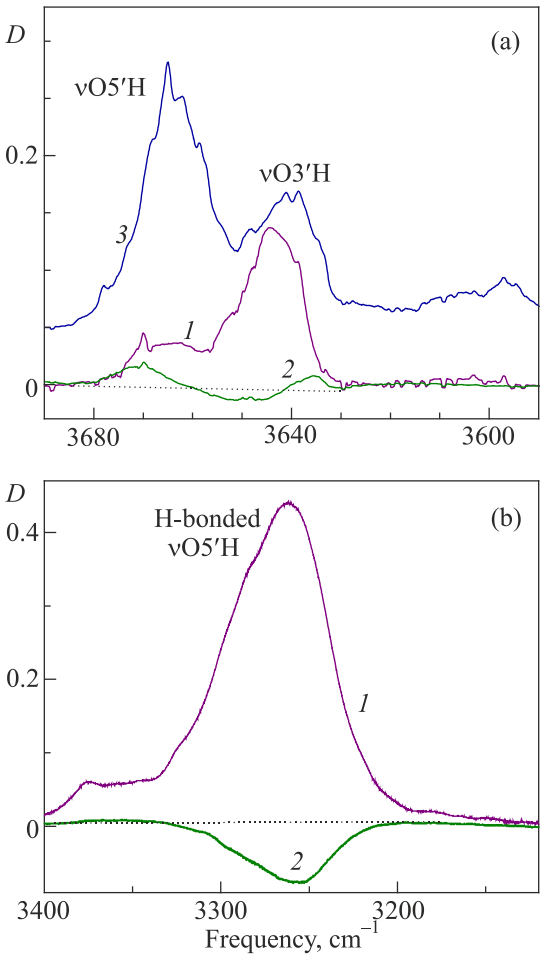

Fig. 24. Experimental FTIR spectra of the region of free (a) and hydrogen-bonded (b) stretching vibrations νOH of 2-deoxyadenosine molecules in an Ar matrix: spectrum after deposition ($T = 6$ K, M/S = = 500) (*1*); difference spectrum after 40 min UV irradiation of matrix sample (*2*); given for comparison, spectrum 2dUr [80] (*3*).

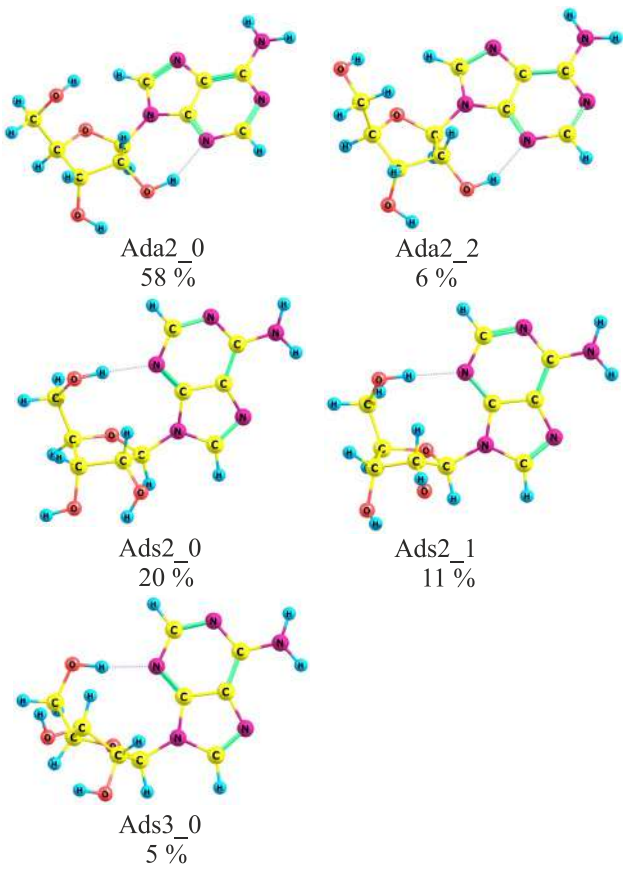

Fig. 25. (Color online) The conformers of Ad that are fixed in the matrix and estimation of their population (%) in the Ar matrices at $T = 6$ K [104].

5.3. Protonated derivatives of guanosine and adenosine in the gas phase

IRMPD spectra of protonated 2′-deoxyguanosine (2dG) and guanosine (Gu) showed that atom N7 is the most favorable protonation site [106]. The most stable structures $[2dG+H]^+$ and $[Gu+H]^+$ *anti*-conformers stabilized by a weak hydrogen bond between C8–H group and atom O5′ [106]. In both cases, the sugar ring is in the C3′-endo conformation. It was also shown that only keto forms of the guanine residue of $[dGuo+H]^+$ and $[Guo+H]^+$ were observed in these experiments [106].

In contrast to 2dG and Gu, 2dA and Ad molecules were protonated at N3 site whereas protonation at N7 was found to be much less favorable [107]. According to the calculated data and IRMPD spectra, only one *syn*-conformation of $[2dA+H]^+$ was observed (Fig. 27) [107]. A similar result was obtained for $[Ad+H]^+$ [107]. This was due to protonation at the N3 site which allowed the formation of a strong intramolecular $N3H^+\bullet\bullet\bullet O5'$ hydrogen bond. It should be noted that the analysis of the experimental spectra did not exclude the presence of trace amount of minor *anti*- and *syn*-conformers of $[2dA+H]^+$ (Fig. 27) and $[Ad+H]^+$ [107]. Obtained data demonstrated significant decrease of quantity of the protonated 2dA and Ad conformers in the gas phase as compared to neutral ones (Figs. 23 and 25).

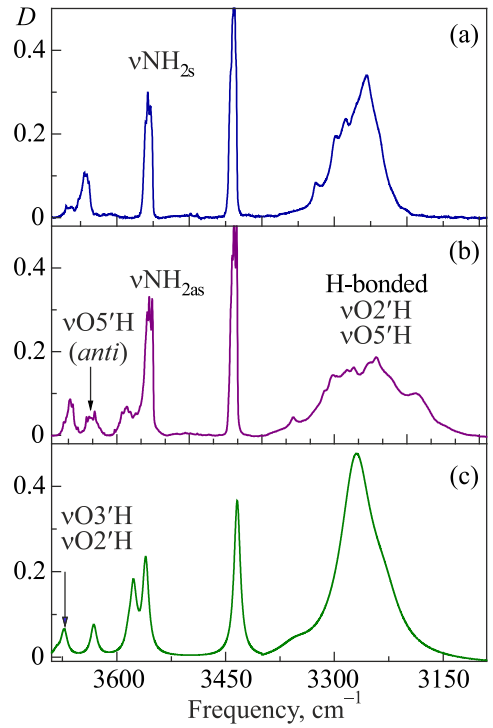

Fig. 26. Experimental and calculated vibrational spectra of the OH, NH stretching vibration region for dA and Ad molecules: (a) dA in an Ar matrix (T = 6 K, M/S = 700); (b) Ad in Ar matrix (T = 6 K, M/S = 600); (c) total spectrum of conformers Ada2_0, Ada2_2, Ads2_0, Ads2_1, Ads3_0, calculated by the DFT/B3LYP/6-311++G(df,pd) method with frequency correction (multiplier 0.951) and taking into account the populations [104].

6. Conclusions

Low temperatures play an important role in the modern highly sensitive spectroscopy of isolated biological molecules. In most methods, the cooling of molecules to cryogenic temperatures occurs directly during the isolation process. It significantly improves the spectral resolution. The cooling rate of is very important in studies of highly flexible biomolecules. The modern methods of action spectroscopy and low-temperature matrix isolation spectroscopy allowed the registration of vibrational spectra of isolated nucleosides in neutral or ionized form. It was shown that pyrimidine and purine nucleosides can be converted into the gas phase by prolonged evaporation from the Knudsen cells without thermal decomposition. Laser evaporation can greatly affect the conformational composition of the gas phase.

The determination of the conformational landscape of nucleosides can be successfully carried out using the relatively simple method DFT/B3LYP/6-31G(d,p). However estimating the energies of individual conformers requires the use of more advanced methods, for example, MP2 with large basis sets. Experimental FTIR spectra of matrix samples are in good agreement with spectra calculated at the DFT/B3LYP/6-311G++(df,pd) or DFT/B3LYP/aug-cc-pVTZ levels of theory. Calculating the energies of protonated structures requires the use of the most sophisticated methods, for example, CCSD(T)/aug-cc-pVTZ.

The conformational equilibrium between *syn*- and *anti*-subsets of pyrimidine and purine nucleosides in the gas

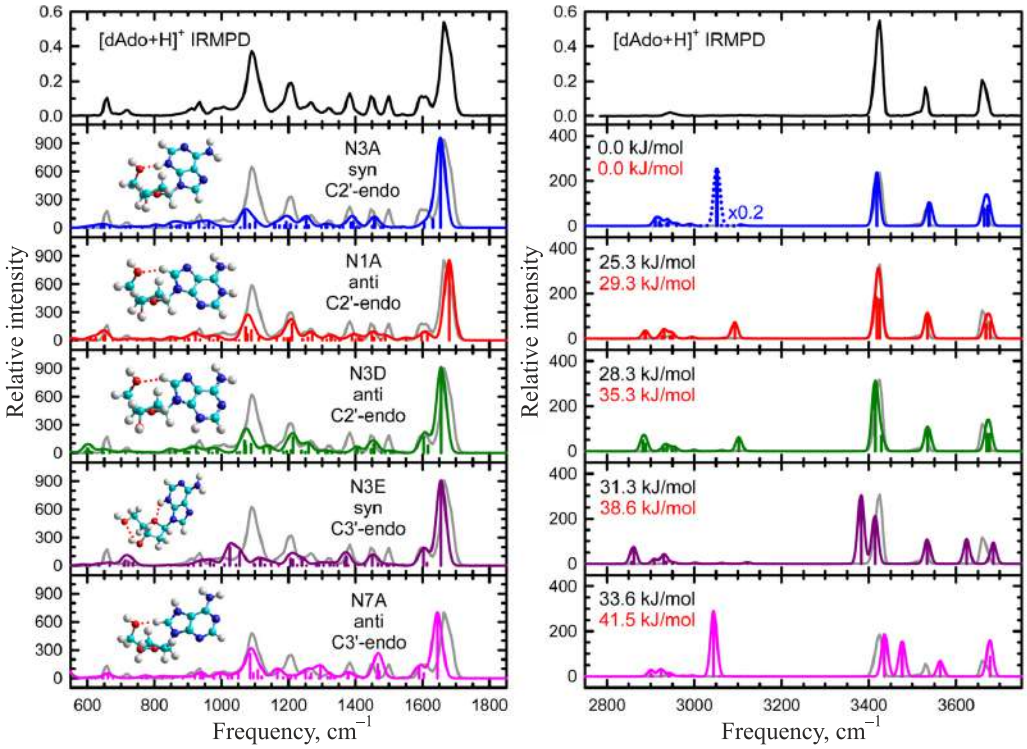

Fig. 27. (Color online) Comparison of the experimental IRMPD action spectrum of $[2dA+H]^+$ with the calculated IR spectra for the low-energy conformers that may be populated in the experiments and the corresponding structures calculated at the B3LYP/6-311+G(d,p) level of theory. The B3LYP/6-311+G(2d,2p) and MP2(full)/6-311+G(2d,2p) relative Gibbs free energies at 298 K are also shown in black and red, respectively. The site of protonation, nucleobase orientation, and sugar puckering are indicated for each conformer [107].

phase is maintained when the molecules are frozen in inert matrices. Interconversion between individual groups of conformers can occur within these subsets upon cooling. In inert matrices at 6 K, the subsets of the *syn*-conformers of deoxyribonucleosides are mostly frozen with the C2'-endo structure of the deoxyribose ring. But the *syn*-conformers of ribonucleosides with the C3′-endo structure of the sugar ring can also be fixed.

Protonation significantly changes the conformational and tautomeric structure of purine and pyrimidine nucleosides. 2,4-dihydroxy forms dominate for protonated derivatives of uridine and thymidine, while *syn*-conformations stabilized by the intramolecular hydrogen bond N3H$^+$•••O5 dominate for adenosine derivatives.

This work was supported by the National Academy of Sciences of Ukraine (under Grant No. 0120U100157).

1. R. Weinkauf, J.-P. Schermann, M. S. de Vries, and K. Kleinermanns, *Eur. Phys. J. D* **20**, 309 (2002).
2. J.-P. Schermann, *Spectroscopy and Modeling of Biomolecular Building Blocks*, Elsevier, Amsterdam (2008). ISBN: 9780444527080
3. J. P. Simons, R. A. Jockusch, P. Carcabal, I. H. Nig, R. T. Kroemer, N. A. MacLeod, and L. C. Snoek, *Int. Rev. Phys. Chem*. **24**, 489 (2005).
4. M. S. de Vries and P. Hobza, *Annu. Rev. Phys. Chem*. **58**, 585 (2007).
5. E. C. Stanca-Kaposta and J. P. Simons, *High-Resolution Infrared–Ultraviolet (IR–UV) Double-Resonance Spectroscopy of Biological Molecules*, in: *Handbook of High-resolution Spectroscopy*, M. Quack and F. Merkt (eds.), John Wiley & Sons, Ltd. (2011). ISBN: 978-0-470-74959-3.
6. *Gas-Phase IR Spectroscopy and Structure of Biological Molecules, Top Curr. Chem*. A. M. Rijs and J. Oomens (eds.), Springer International Publishing Switzerland (2015), Vol. 364.
7. *Nucleic Acid in the Gas Phase, Physical Chemistry in Action,* V. Gabelica (ed.), Springer-Verlag, Berlin, Heidelberg (2014).
8. N. C. Polfer and J. Oomens, *Phys. Chem. Chem. Phys*. **9**, 3804 (2007).
9. N. C. Polfer and J. Oomens, *Mass Spectr. Rev.* **28**, 468 (2009).
10. K. Schwing and M. Gerhards, *Intern. Rev. Phys. Chem.* **35**, 569 (2016).
11. S. Bakels, M.-P. Gaigeot, and A. M. Rijs, *Chem. Rev*. **120**, 3233 (2020).
12. P. Maitre, D. Scuderi, D. Corinti, B. Chiavarino, M. E. Crestoni, and S. Fornarini, *Chem. Rev*. **120**, 3261 (2020).
13. E. Herbst and E. F. van Dishoeck, *Annu. Rev. Astron. Astrophys*. **47**, 427 (2009).
14. S. Kwok, *Astron. Astrophys. Rev*. **24**, 8 (2016).
15. S. A. Sandford, M. Nuevo, P. P. Bera, and T. J. Lee, *Chem. Rev*. **120**, 4616 (2020).
16. E. D. Radchenko, G. G. Sheina, N. A. Smorygo, and Y. P. Blagoi, *J. Mol. Struct*. **116**, 387 (1984).
17. M. Szczesniak, K. Szczepaniak, J. S. Kwiatkowski, K. KuBulat, and W. B. Person, *J. Am. Chem. Soc*. **110**, 8319 (1988).
18. S. Cradock and A. J. Hinchliffe, *Matrix Isolation*, Cambridge University Press, New York (1975).
19. J. Oomens, B. G. Sartakov, G. Meijer, and G.von Helden, *Inter. J. Mass Spectr*. **254**, 1 (2006).
20. C. Callegari, K. K. Lehmann, R. Schmied, and G. Scoles, *J. Chem. Phys*. **115**, 1090 (2001).
21. J. P. Toennies and A. F. Vilesov, *Angew. Chem. Int. Ed*. **43**, 2622 (2004).
22. D. Verma, R. M. P. Tanyag, S. M. O. O'Connell, and A. F. Vilesov, *Adv. Phys. X* **4**, 1553569 (2019).
23. W. Saenger, *Principles of Nucleic Acids Structure*, Springer-Verlag, New York (1984).
24. L. P. Jordheim, D. Durante, F. Zoulim, and C. Dumontet, *Nature Rev. Drug Disc*. **12**, 447 (2013).
25. S. A. Krasnokutski, A. Yu. Ivanov, V. Izvekov, G. G. Sheina, and Yu. P. Blagoi, *J. Mol. Struct*. **482–483**, 249 (1998).
26. A. M. Rijs and J. Oomens, *IR Spectroscopic Techniques to Study Isolated Biomolecules*, in: *Gas-Phase IR Spectroscopy and Structure of Biological Molecules*, A. Rijs and J. Oomens (eds.), *Top. Curr. Chem.*, Springer (2015), Vol. 364.
27. F. Huisken, *Infrared Vibrational Predissociation Spectroscopy of Small Size-Selected Clusters*, in: *Adv. Chem. Phys*, I. Prigogine and S. A. Rice (eds.), *Adv. Chem. Phys*. (1992), Vol. LXXXI. ISBN 0-471-54570-8
28. R. Frochtenicht, M. Kaloudis, M. Koch, and F. Huisken, *J. Chem. Phys*. **105**, 6128 (1996).
29. F. Huisken, O. Werhahn, A. Y. Ivanov, and S. A. Krasnokutski, *J. Chem. Phys*. **111**, 2978 (1999).
30. V. Yatsyna, D. J. Bakker, P. Salén, R. Feifel, A. M. Rijs, and V. Zhaunerchyk, *Phys. Rev. Lett*. **117**, 118101 (2016).
31. V. Yatsyna, *Structure-Specific Vibrational Modes of Isolated Biomolecules Studied with Mid- and Far-Infrared Laser Spectroscopy*, Ph. D. Thesis, University of Gothenburg, Sweden (2019).
32. T. R. Rizzo and O. V. Boyarkin, *Cryogenic Methods for the Spectroscopy of Large, Biomolecular Ions*, in: *Gas-Phase IR Spectroscopy and Structure of Biological Molecules,* A. Rijs and J. Oomens (eds.), *Top. Curr. Chem.*, Springer (2015), Vol. 364.
33. V. Gabelica and F. Rosu, *Gas-Phase Spectroscopy of Nucleic Acids*, in: *Nucleic Acid in the Gas Phase, Physical Chemistry in Action*, V. Gabelica (ed.), Springer-Verlag, Berlin, Heidelberg (2014).
34. F. Filsinger, D. S. Ahn, G. Meijer, and G. von Helden, *Phys. Chem. Chem. Phys*. **14**, 13370 (2012).
35. D. A. Thomas, R. Chang, E. Mucha, M. Lettow, K. Greis, S. Gewinner, W. Schollkopf, G. Meijer, and G. von Helden, *Phys. Chem. Chem. Phys*. **22**, 18400 (2020).
36. E. Garand, *J. Phys. Chem. A* **122**, 6479 (2018).
37. K. C. Fischer, S. L. Sherman, J. M. Voss, J. Zhou, and E. Garand, *J. Phys. Chem*. **123**, 3355 (2019).
38. J. J. Scherer, J. B. Paul, A. O'Keefe, and R. J. Saykally, *Chem. Rev*. **97**, 25 (1997).

39. R. N. Casaes, J. B. Paul, R. P. McLaughlin, R. J. Saykally, and T. van Mourik, *J. Phys. Chem. A* **108**, 10989 (2004).
40. J. L. Alonso and J. C. Lopez, *Microwave Spectroscopy of Biomolecular Building Blocks*, in: *Gas-Phase IR Spectroscopy and Structure of Biological Molecule,* A. Rijs and J. Oomens (eds.), *Top. Curr. Chem.*, Springer (2015), Vol. 364.
41. I. Pena, C. Cabezas, and J. L. Alonso, *Angew. Chem. Int. Ed.* **54**, 2991 (2015).
42. A. Yu. Ivanov, A. M. Plokhotnichenko, E. D. Radchenko, G. G. Sheina, and Yu. P. Blagoi, *J. Mol. Struct.* **372**, 91 (1995).
43. A. Yu. Ivanov and A. M. Plokhotnichenko, *Instr. Experim. Techn.* **52**, 308 (2009).
44. A. Yu. Ivanov, S. A. Krasnokutski, G. G. Sheina, and Yu. P. Blagoi, *Spectrochim. Acta A* **59**, 1959 (2003).
45. A. Yu. Ivanov, S. A. Krasnokutski, and G. G. Sheina, *Fiz. Nizk. Temp.* **29**, 1065 (2003) [*Low Temp. Phys.* **29**, 809 (2003)].
46. A. Yu. Ivanov and V. A. Karachevtsev, *Fiz. Nizk. Temp.* **33**, 772 (2007) [*Low Temp. Phys.* **33**, 590 (2007)].
47. A. Kovacs and A. Yu. Ivanov, *J. Phys. Chem. B* **113**, 2151 (2009).
48. P. Felder and Hs. H. Gunthard, *Chem. Phys.* **71**, 9 (1982).
49. U. Erlekam, M. Frankowski, G. von Helden, and G. Meijer, *Phys. Chem. Chem. Phys.* **9**, 3786 (2007).
50. P. D. Godfrey, R. D. Brown, and F. M. Rodgers, *J. Mol. Struct.* **376**, 65 (1996).
51. P. D. Godfrey and R. D. Brown, *J. Am. Chem. Soc.* **120**, 10724 (1998).
52. R. S. Ruoff, T. D. Klots, T. Emilsson, and H. S. Gutowsky, *J. Chem. Phys.* **93**, 3142 (1990).
53. J. H. Jensen and M. S. Gordon, *J. Am. Chem. Soc.* **113**, 7917 (1991).
54. I. D. Reva, S. G. Stepanian, L. Adamowicz, and R. Fausto, *Chem. Phys. Lett.* **374**, 631 (2003).
55. A. J. Barnes, *J. Mol. Struct.* **113**, 161 (1984).
56. M. Poliakoff and J. J. Turner, *Infrared Laser Photochemistry in Matrices,* in: *Chemichal and Biochemical Applications of Lasers*, C. Bradley Moor (ed.), Academic Press, New York (1980).
57. *Cryocrystals*, B. I. Verkin and A. F. Prihotko (eds.), Naukova Dumka, Kiev (1983). [in Russian].
58. M. P. Gaigeot, N. Leulliot, M. Ghomi, H. Jobic, C. Coulombeau, and O. Bouloussa, *Chem. Phys.* **261**, 217 (2000).
59. N. Leulliot, M. Ghomi, H. Jobic, O. Bouloussa, V. Baumruk, and C. Coulombeau, *J. Phys. Chem. B* **103**, 10934 (1999).
60. A. Hocquet and M. Ghomi, *Phys. Chem. Chem. Phys.* **2**, 5351 (2000).
61. O. V. Shishkin, A. Pelmenschikov, D. M. Hovorun, and J. Leszczynski, *J. Mol. Struct.* **526**, 329 (2000).
62. A. Hocquet, *Phys. Chem. Chem. Phys.* **3**, 3192 (2001).
63. N. Leulliot, M. Ghomi, G. Scalmani, and G. Berthier. *J. Phys. Chem. A* **103**, 8716 (1999).
64. C. Altona and M. Sundaralingam, *J. American Chem. Soc.* **94**, 8205 (1972).
65. Y. P. Yurenko, R. O. Zhurakivsky, M. Ghomi, S. P. Samijlenko, and D. M. Hovorun, *J. Phys. Chem. B* **111**, 6263 (2007).
66. Y. P. Yurenko, R. O. Zhurakivsky, M. Ghomi, S. P. Samijlenko, and D. M. Hovorun, *J. Phys. Chem. B* **111**, 9655 (2007).
67. Y. P. Yurenko, R. O. Zhurakivsky, M. Ghomi, S. P. Samijlenko, and D. M. Hovorun, *J. Phys. Chem. B* **112**, 1240 (2007).
68. R. O. Zhurakivsky and D. M. Hovorun, *Ukrainica Bioorganica Acta* **2**, 56 (2006). [in Ukranian].
69. R. O. Zhurakivsky and D. M. Hovorun, *Biopolymer and Cell* **24**, 142 (2008). [in Ukranian].
70. R. O. Zhurakivsky and D. M. Hovorun, *Biopolymer and Cell* **23**, 45 (2007). [in Ukranian].
71. R. O. Zhurakivsky and D. M. Hovorun, *Biopolymer and Cell* **23**, 365 (2007). [in Ukranian].
72. R. O. Zhurakivsky and D. M. Hovorun, *Ukrainica Bioorganica Acta* **2**, 44 (2007). [in Ukranian].
73. Gaussian 16, Revision B.01, M. J. Frisch, G. W. Trucks, H. B. Schlegel, G. E. Scuseria, M. A. Robb, J. R. Cheeseman, G. Scalmani, V. Barone, G. A. Petersson, H. Nakatsuji, X. Li, M. Caricato, A. V. Marenich, J. Bloino, B. G. Janesko, R. Gomperts, B. Mennucci, H. P. Hratchian, J. V. Ortiz, A. F. Izmaylov, J. L. Sonnenberg, D. Williams-Young, F. Ding, F. Lipparini, F. Egidi, J. Goings, B. Peng, A. Petrone, T. Henderson, D. Ranasinghe, V. G. Zakrzewski, J. Gao, N. Rega, G. Zheng, W. Liang, M. Hada, M. Ehara, K. Toyota, R. Fukuda, J. Hasegawa, M. Ishida, T. Nakajima, Y. Honda, O. Kitao, H. Nakai, T. Vreven, K. Throssell, J. A. Montgomery, Jr., J. E. Peralta, F. Ogliaro, M. J. Bearpark, J. J. Heyd, E. N. Brothers, K. N. Kudin, V. N. Staroverov, T. A. Keith, R. Kobayashi, J. Normand, K. Raghavachari, A. P. Rendell, J. C. Burant, S. S. Iyengar, J. Tomasi, M. Cossi, J. M. Millam, M. Klene, C. Adamo, R. Cammi, J. W. Ochterski, R. L. Martin, K. Morokuma, O. Farkas, J. B. Foresman, and D. J. Fox, Gaussian, Inc., Wallingford CT, (2016).
74. Alex A. Granovsky, *Firefly Version 7.1.G,* (2009).
75. M. W. Schmidt, K. K. Baldridge, J. A. Boatz, S. T. Elbert, M. S. Gordon, J. H. Jensen, S. Koseki, N. Matsunaga, K. A. Nguyen, S. Su, T. L. Windus, M. Dupuis, and J. A. Montgomery, *J. Comput. Chem.* **14**, 1347 (1993).
76. A. D. Becke, *Phys. Rev. A* **38**, 3098 (1988).
77. T. H. Dunning, Jr., *J. Chem. Phys.* **90**, 1007 (1989).
78. S. Grimme, J. Antony, S. Ehrlich, and H. Krieg, *J. Chem. Phys.* **132**, 154104 (2010).
79. S. Grimme, S. Ehrlich, and L. Goerigk, *J. Comput. Chem.* **32**, 1456 (2011).
80. A. Yu. Ivanov, *Fiz. Nizk. Temp.* **40**, 727 (2014) [*Low Temp. Phys.* **40**, 565 (2014)].
81. A. Yu. Ivanov, Yu. V. Rubin, S. A. Egupov, L. F. Belous, and V. A. Karachevtsev, *Fiz. Nizk. Temp.* **39**, 704 (2013) [*Low Temp. Phys.* **39**, 546 (2013)].
82. A. Yu. Ivanov, *Fiz. Nizk. Temp.* **34**, 962 (2008) [*Low Temp. Phys.* **34**, 762 (2008)].
83. A. Yu. Ivanov, S. G. Stepanian, V. A. Karachevtsev, and L. Adamowicz, *Fiz. Nizk. Temp.* **45**, 1181 (2019) [*Low Temp. Phys.* **45**, 1008 (2019)].

84. A. Yu. Ivanov, *Fiz. Nizk. Temp*. **36**, 571 (2010) [*Low Temp. Phys*. **36**, 458 (2010)].
85. S. Ptasinska, P. Candori, S. Denifl, S. Yoon, V. Grill, P. Scheier, and T. D. Mark, *Chem. Phys. Lett*. **409**, 270 (2005).
86. H. Levola, K. Kooser, E. Rachlew, E. Nommiste, and E. Kukk, *Int. J. Mass Spectrom*. **353**, 7 (2013).
87. A. Yu. Ivanov, Yu. V. Rubin, S. A. Egupov, L. F. Belous, and V. A. Karachevtsev, *Fiz. Nizk. Temp*. **40**, 1409 (2014) [*Low Temp. Phys.* **40**, 1097 (2014)].
88. R. R. Wu, Bo Yang, C. E. Frieler, G. Berden, J. Oomens, and M. T. Rodgers, *Phys. Chem. Chem. Phys*. **17**, 25978 (2015).
89. R. R. Wu, Bo Yang, C. E. Frieler, G. Berden, J. Oomens, M. T. Rodgers, *J. Am. Soc. Mass Spectrom*. **27**, 410 (2016).
90. J.-Y. Salpin and D. Scuderi, *Rapid Commun. Mass Spectrom.* **29**, 1898 (2015).
91. Y. Zhu, H. A. Roy, N. A. Cunningham, S. F. Strobehn, J. Gao, M. U. Munshi, G. Berden, J. Oomens, and M. T. Rodgers, *J. Am. Soc. Mass Spectrom*. **28**, 2423 (2017).
92. A. Filippi, C. Fraschetti, F. Rondino, S. Piccirillo, V. Steinmetz, L. Guidoni, and M. Speranza, *Int. J. Mass Spectrom*. **354–355**, 54 (2013).
93. R. R. Wu, B. Yang, C. E. Frieler, G. Berden, J. Oomens, and M. T. Rodgers, *J. Phys. Chem. B* **119**, 5773 (2015).
94. J.-Y. Salpin, S. Guillaumont, J. Tortajada, L. MacAleese, J. Lemaire, and P. Maitre, *Chem. Phys. Chem*. **8**, 2235 (2007).
95. J. M. Bakker, R. K. Sinha, T. Besson, M. Brugnara, P. Tosi, J.-Y. Salpin, and P. Maitre, *J. Phys. Chem. A* **112**, 12393 (2008).
96. E. Nir, P. Imhof, K. Kleinermanns, and M. S. de Vries, *J. Am. Chem. Soc*. **122**, 8091 (2000).
97. E. Nir, Ch. Plutzer, K. Kleinermanns, and M. de Vries, *Eur. Phys. J. D* **20**, 317 (2002).
98. E. Nir, I. Hunig, K. Kleinermanns, and M. S. de Vries, *Chem. Phys. Chem*. **5**, 131, (2004).
99. A. Abo-Riziq, B. O. Crews, I. Compagnon, J. Oomens, G. Meijer, G. Von Helden, M. Kabelac, P. Hobza, and M. S. de Vries, *J. Phys. Chem. A* **111**, 7529 (2007).
100. M. S. de Vries, *Top. Curr. Chem.*, Springer, (2014), Vol. 364.
101. E. Nir and M. S. de Vries, *Int. J. Mass Spectrom*. **219**, (2002).
102. G. C. P. van Zundert, S. Jaeqx, G. Berden, J. M. Bakker, K. Kleinermanns, J. Oomens, and A. M. Rijs, *Chem. Phys. Chem*. **12**, 1921 (2011).
103. D. Tuna, A. L. Sobolewski, and W. Domcke, *J. Phys. Chem. A* **118**, 122 (2014).
104. A. Yu. Ivanov, Yu. V. Rubin, S. A. Egupov, L. F. Belous, and V. A. Karachevtsev, *Fiz. Nizk. Temp*. **41**, 1198 (2015) [*Low Temp. Phys*. **41**, 936 (2015)].
105. Y. Tanaka, *Thermochim. Acta* **144**, 177 (1989).
106. R. R. Wu, Bo Yang, G. Berden, J. Oomens, and M. T. Rodgers, *J. Phys. Chem. B* **118**, 14774 (2014).
107. R. R. Wu, Bo Yang, G. Berden, J. Oomens, and M. T. Rodgers, *J. Phys. Chem. B* **119**, 2795 (2015).

Молекулярна структура та коливальні спектри ізольованих нуклеозидів при низьких температурах
(Огляд)

A. Yu. Ivanov, S. G. Stepanian

Розглянуто застосування різних методів “action spectroscopy” та спектроскопії поглинання для дослідження структури біологічних молекул та їх складових фрагментів в ізольованому стані. Основну увагу приділено результатам, що досягнуті у вивченні нуклеозидів, які є структурними одиницями ДНК, РНК. Продемонстровано, що сучасні методи спектроскопії з використанням низьких температур дозволяють реєструвати коливальні спектри ізольованих нуклеозидів в нейтральній або іонізованої формі. Показано, що деякі нуклеозиди можуть бути переведені в газову фазу шляхом тривалого випаровування з комірки Кнудсена без термічного розкладання. Охолодження молекул до кріогенних температур грає важливу роль в цих дослідженнях. Завдяки швидкому охолодженню конформаційна рівновага газової фази між *син*- та *анти*- підмножинами нуклеозидів зберігається при заморожуванні в інертних матрицях. Усередині цих підмножин можуть відбуватися процеси інтерконверсії між низько бар’єрними конформерами при охолодженні. В інертних матрицях при 6 К підмножини *син*-конформерів дезоксірибонуклеозидів в основному заморожуються з C2′-ендо- структурою дезоксірибозного кільця. Структури молекулярних іонів нуклеозидів сильно відрізняються від їх нейтральних форм. Зокрема протонування призводить до домінування енольних форм тимідину, а також *син*-конформацій аденозину, які стабілізовані внутрішньомолекулярним водневим зв’язком $N3H^+$ ••• O5.

Ключові слова: ІЧ Фур’є-спектроскопія, низькотемпературна матрична ізоляція, нуклеозиди, *ab initio* розрахунки.